Received 11 May 2023; revised 29 June 2023; accepted 3 July 2023. Date of publication 7 July 2023; date of current version 27 July 2023.

Digital Object Identifier 10.1109/OJAP.2023.3293123

Receive Mode Time-Modulated Antenna Array Incorporating Subsampling—Theoretical Concept and Laboratory Investigation

EDWARD A. BALL (Member, IEEE), SUMIN DAVID JOSEPH, AND ALAN TENNANT

Communications Research Group, Department of Electronic and Electrical Engineering, The University of Sheffield, S10 2TN Sheffield, U.K.

CORRESPONDING AUTHOR: E. A. BALL (e-mail: e.a.ball@sheffield.ac.uk)

This work was supported by the U.K. Research and Innovation (UKRI) Future Leaders Fellowship under Grant MR/T043164/1.

ABSTRACT An eight element Subsampling Time Modulated Array (STMA) operating in receive mode with a carrier at 2.4 GHz is presented and demonstrated using bespoke Radio Frequency (RF) hardware. Each STMA cell incorporates subsampling functionality, with the sampling frequency significantly below the carrier frequency and requiring minimal additional hardware. By using this concept, the hardware required for a receiver incorporating an antenna array can be reduced and costs saved. STMA design equations and architecture strategies are presented, and a prototype hardware demonstrator is introduced. Laboratory measurements confirm that a received radiated signal, arranged to use the fundamental or a harmonic beam pointed at the radiating source, can be resolved from the subsampled intermediate frequency (IF) output. The concept demonstration hardware provides a measured array conversion gain of 11.4 dBi on the boresight beam, 7.8 dBi on the first positive and 11.3 dBi on the first negative harmonic beams, as resolved at the final combined IF output. The array IF output Signal to Noise and Distortion ratio is 69 dB. The dependence of array sidelobe level performance on STMA sampling switch rise time is also uncovered, though good performance with real, imperfect, hardware is still obtained.

INDEX TERMS Microwave circuits, RF hardware platform, time-modulated antenna arrays (TMAs), signal sampling.

I. INTRODUCTION

THE DESIGN of the antenna array is always an important aspect of a radio communications system. The global adoption of 5G mobile communications continues, with over 1.3 billion connections worldwide [1]. Stimulated by this market, there continues to be significant research opportunities for 5G and future 6G systems, including mmWave [2], though often with a focus on massive MIMO for sub 6 GHz systems [3]. Propagation channels are often sparse at mmWave frequencies, so simple phased array antenna structures remain very relevant. Phased arrays systems are also important for many commercial and military communications scenarios at microwave frequencies.

The Time Modulated Array (TMA) [4], [5], [6], [7], [8] is a novel class of antenna array that does not use conventional phase shifters or vector modulators to apply a phase shift to each array radiating element. Instead, simple RF switching techniques are used, with simple controlling waveforms. Fourier analysis of the switch control waveforms reveals a phase shifting property that results in an element-specific phase shift at the carrier, as required to realise a phased array. The TMA can be used in transmit (TX) or receive (RX) arrays and can also handle multiple beams of different data (e.g., for different target users) [9], [10], [11], diversity reception [12] or supporting polarization diversity [13]. The TMA can also be used to steer a null to minimise interference from an unwanted source [14], [15], [16], [17].

A TMA can be used in direction finding systems [18], [19] and radar systems [20], [21]. It has also been demonstrated that data transport using the harmonic beams and a radar function using the boresight beam can be supported [22], [23], [24], [25]. The TMA can also be used in reflector

array applications [26], [27] or for generating circular polarization [28], [29] and for generating orbital angular momentum waves [30].

TMA hardware has historically been implemented using RF switches. Recent improved switch and control technologies have enabled improved RF bandwidth performance [31]. However, other advanced techniques using more RF hardware have adopted single sideband and IQ modulation to offer high RF performance [32], with some related hardware simplifications also investigated [33].

The TMA non-steered boresight beam results from the Fourier DC component (due to a non-zero average) of the switch control waveform. Recent work has shown that this boresight beam can be attenuated using simple hardware and digital control waveforms [34].

The TMA has also been demonstrated at mmWave frequencies, for secure communications applications [35]. As evidenced by the above examples, the TMA concept supports many useful and novel applications and remains important.

Although multiple concurrent harmonic beams can be generated by the TMA, the resulting beam magnitudes decrease with increasing harmonic [34]. In practice, most published works use just the boresight beam, first or second harmonic beams. The control of the TMA beams and their sidelobes is a major topic of research, such as in addressing suppression of sidelobes and sidebands [36].

The TMA is often considered in isolation from the communication system, with an RF carrier input that is processed by the TMA and results in steered beams, such as for an IoT system [37].

Software Defined Radio (SDR) applied to phased array beamforming has been researched over many years [38]. Analogue beamformers (ABF) require controllable phase shifters, such as [39] at 25 – 31 GHz and variable gain amplifiers (VGA), such as [40] at 22.8 – 35 GHz. ABFs have also now been realized in integrated front-end devices, such as [41] offering a four-element transceiver at 33.5 – 37.5 GHz. In [42] a four element 36 – 40 GHz ABF is realized for 5G. Other recent works in mmWave ABF include a single channel transceiver RF front-end [43], and quad-channel front-end [44]. Integrated, Digital Beamformer (DBF) systems have also been demonstrated, such as a 16 element RX [45]. TMA concepts have recently been applied to generate mmWave MIMO at 26 – 33 GHz through switching the LNA current, though the system still requires a VGA and phase shifter in an initial ABF stage [46].

However, to the best of the authors' knowledge, there is no reported work that incorporates the TMA directly within a SDR inspired downconverter with the intention to simplify overall hardware – which is stimulus and the focus of the work in this paper. By combining the carrier down conversion within the TMA operation, there exists the possibility to simplify and reduce cost in an SDR system. Although we demonstrate the principle in a RX array, it could also be applicable to a TX system, with appropriate circuit modification and filtering.

RX SDR systems commonly make use of an ADC to sample and digitize the RF signal. The sampling action generates Nyquist bands and it is well known that an RF signal presented in a higher Nyquist (alias) band can thus be down converted by subsampling via these sampling aliases [47], [48]. The sampling action can be considered separately from the digitization action and thus a dedicated sampler circuit can be used to perform the subsampling down conversion. The zero-order hold that would typically be the basis of such a circuit can be theoretically approximated by a simple ideal switch and sample hold capacitor. It is this concept that stimulates our work into combining a switch-based TMA with a sampler to form a single subsampler down converting TMA system. Hence, the key contributions of this paper are as follows:-

- Theoretical introduction of an RX subsampling TMA, leading to the new STMA concept,
- Theoretical performance predictions of the STMA and identification of key design criteria,
- Laboratory measured results from a 2.4 GHz hardware RX STMA prototype, compared to theoretical predictions.

The paper continues with the STMA concept and prototype described in Section II, then the prototype tests and verification of the hardware platform is presented in Section III. Chamber radiated antenna pattern measurements are presented in Section IV and an overall discussion of findings in Section V. The paper concludes in Section VI.

II. SUBSAMPLING TMA CONCEPT

Since many modern radio systems are based on a SDR approach, it is interesting to consider how the TMA could directly apply SDR concepts and thus reduce hardware complexity and cost. In a conventional approach, the output of a passive RX antenna array may first be down converted to an IF and then sampled directly by an ADC and this is a widely used technique. When considering such a conventional sampler approach applied to the TMA output, it becomes interesting to consider what happens if the sampler gate is moved forward in the signal chain. Fig. 1 shows the sampler moved forward from the ADC / array interface and is now next to the TMA switches. Clearly, this is only an intuitive step and would be expensive in practice, but it is useful illustratively.

The subsequent step is to consider how the TMA switch and the sampler could be combined into one switch circuit function. In practice this is a relatively simple step, as represented in Fig. 2, which shows that by repurposing the already used TMA switch and addition of a hold circuit (a capacitor) the TMA can now perform the dual role of TMA and subsampler, though with a more complex control waveform required. The STMA concept thus makes use of the existing RF switch, as already required by the TMA, and a relatively simple addition to the circuitry to

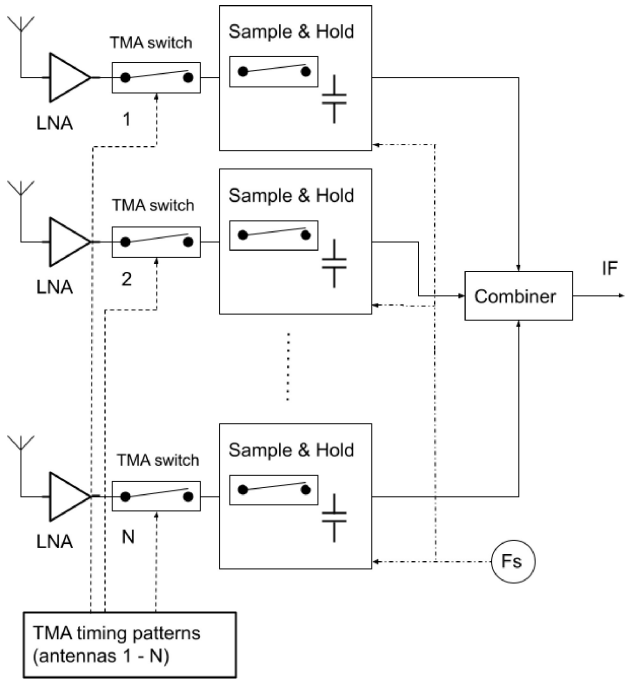

FIGURE 1. Illustrative concept - each TMA switching cell is followed by sampler, sampling at *Fs*.

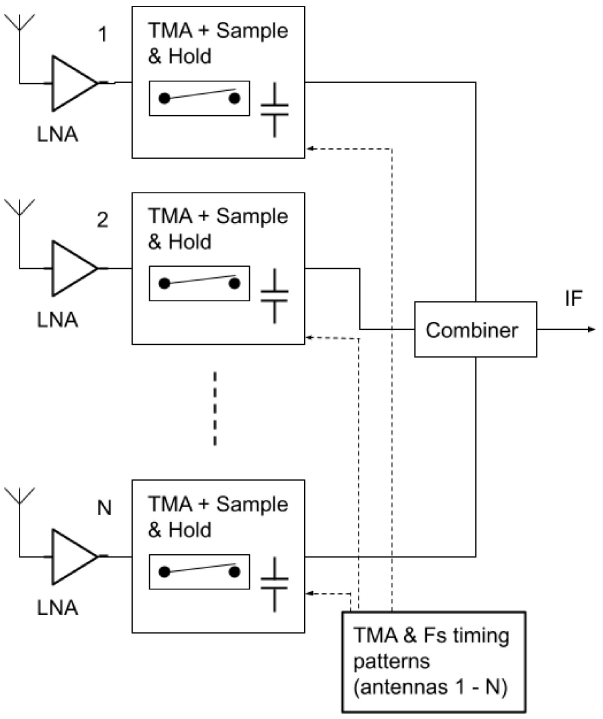

FIGURE 2. TMA and sampler function combined.

support sampling. However, as will be discussed later, the RF requirements of this combined function switch are now more demanding.

One issue is the maximum analogue bandwidth supported by the STMA switch, which must pass the incoming RF carrier signal and also switch at the desired sampling

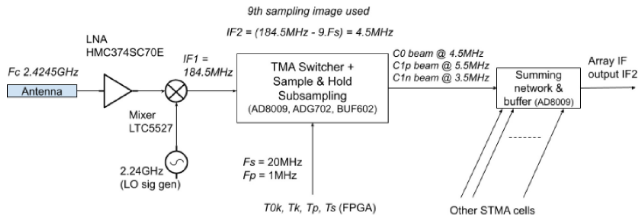

FIGURE 3. RX STMA concept demonstrator with frontend mixer down conversion.

rate *Fs*. The optimal design of this switch is worthy of further research, but for expediency this article makes use of standard off the shelf parts to demonstrate STMA concepts.

A. STMA RX PROTOTYPE CIRCUIT

In our demonstrator design we use an antenna array at 2.4 GHz and initially down convert using a conventional RF mixer to *IF1*, creating an IF signal suitable for the switches' limited input RF bandwidth (BW), as illustrated in Fig. 3.

If higher BW switches had been available this initial mixing stage would not be required.

After the TMA and subsampling operation, *IF2* is produced as the final output from the system. In the demonstrator, the carrier frequency F_c is 2.2425 GHz, *IF1* is 184.5 MHz and *IF2* is centred on 4.5 MHz. To achieve this, the TMA frame period *Tp* is 1 μs and the subsampler frequency *Fs* is 20 MHz (related design equations are presented later).

This two-stage (mixer first) conceptual approach could also be employed more generally if needed, such as at mmWave frequencies. This would allow the initial down conversion to be implemented using pragmatic low power and simple mixer technology and then employing the STMA at IF frequencies, where device switch technologies are more practical.

To demonstrate the STMA concept requires a practical hardware implementation. The choice of sampler switch dictates the maximum design frequencies for analogue BW and sampling rate and so defines the system.

Our demonstration prototype employs an Analog Devices ADG702 analogue switch [49] which has a 3 dB BW of circa 250 MHz thus defining the maximum upper limit for *IF1*. The conceptual block diagram of the prototype system at 2.4 GHz is presented in Fig. 3, with detail for one STMA cell. The full circuit diagram of one STMA cell is presented in Fig. 4, with eight copies used in the demonstrator system, integrated and combined as shown in Fig. 5.

The design of the STMA cell incorporates several important RF circuit aspects which will now be discussed, with reference to Fig. 4. The 2.4 GHz RX signal path from the antenna starts with the Analog Devices HMC374 [50] Low Noise Amplifier (LNA) U5 and then feeds the down conversion mixer LT5527 [51] U3. The mixer LO (local oscillator) is provided through a corporate feed network on the PCB, feeding all the mixers from a single LO signal generator. Mixer U3 requires a 50 Ω termination at its *IF1* output and

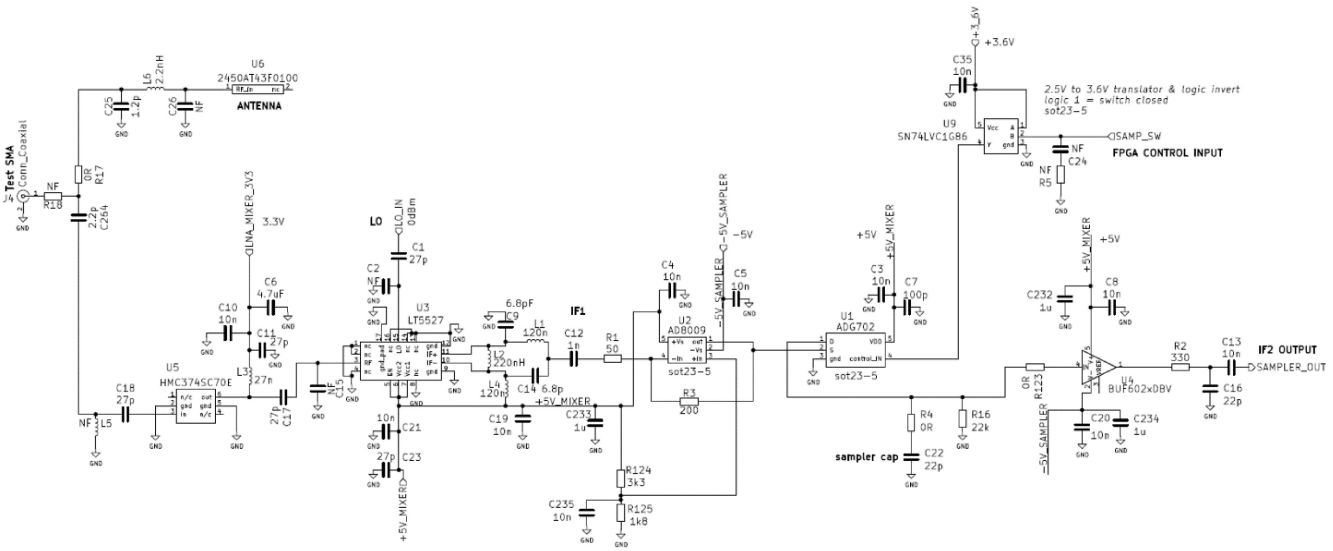

FIGURE 4. Circuit diagram of one STMA RX cell (antenna or test connector input to IF2 output).

this is provided by U2, a AD8009 [52] high BW opamp acting as an inverting amplifier and also conceptually translating the circuit operation from RF power signals from the antenna side to voltage signals as required by the sampler. In the U2 inverting amplifier stage resistor R1 provides the 50 Ω termination for the mixer, with a stage voltage gain of 12 dB. U2 also provides a low impedance drive to the ADG702 switch U1, which is important to help achieve a fast charge-up time for the sampling capacitor C22. U1 and C22 form the core of the STMA, performing both the array phase shifting and subsampling.

The ADG702 switch has an on resistance of 2 Ω and the AD8009 has an output impedance of circa 0.5 Ω, leading to a combined series resistance of circa 2.5 Ω at 4.5 MHz (centre of *IF2*) supplying C22. The output from the sampler capacitor C22 must also be buffered to minimise discharge when the ADG702 switch is in its isolation (off) state. U4 is used as the buffer; a Texas Instruments BUF602 [53] with 1 MΩ input impedance. At the output of the STMA cell, the *IF2* signal from U4 is then combined with the outputs from the other STMA cells using a AD8009 inverting opamp with 50 Ω output impedance and an eight-input resistive combiner, as shown in simplified form in Fig. 5. Note that the output is now at the subsampled signal *IF2*, not the carrier F_c or *IF1*.

In general switch U1, when used as a sampler, must provide a very high impedance in the off state and a very low impedance in the on state (high output drive current capability) as well as fast switching. This is to ensure the 'hold' capacitor C_{samp} (C22) charges quickly when the switch is enabled and then discharges only very slowly (ideally not at all) whilst the switch is off. It is desirable to only 'blip' the switch on, so it only samples the incoming signal for the briefest possible duration, as an approximation to a sampling impulse.

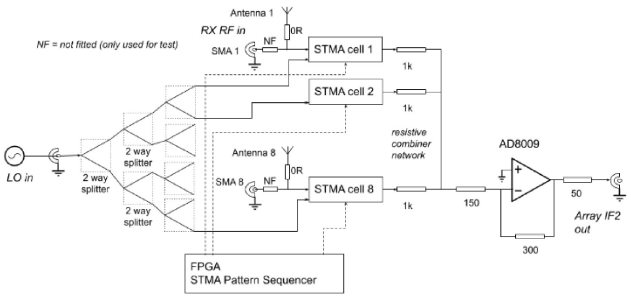

FIGURE 5. Integration of 8 STMA cells into full STMA RX system (simplified representation).

The simple sampler R-C circuit based around C_{samp} must be considered in terms of its charge-up time and its hold time. The charge-up time constant T_{charge} can be approximated by (1), where C_{samp} corresponds to C22 and equals 22 pF, ADG702 $Rswitch_{ON}$ is 2 Ω and AD8009 $Rout_{opamp}$ is 0.5 Ω.

$$T_{charge} = C_{samp}\left(Rout_{opamp} + Rswitch_{ON}\right) \tag{1}$$

The discharge time constant T_{hold} can be approximated by (2), where Rp is the parallel combination of 1 MΩ due to the BUF602 input and the R16 value of 22 kΩ.

$$T_{hold} = C_{samp}R_p \tag{2}$$

The ADG702 has a 10 pA leakage current when in signal isolation (off) state, so is not expected to significantly discharge C_{samp}. Hence, for the proposed circuit values T_{charge} = 55 ps and T_{hold} = 484 ns. Thus, the capacitor is expected to charge to 5 time constants in 275 ps, which is 0.55% of the sample rate period (since Fs = 20 MHz). In hold mode, with the ADG702 switch in isolation (off) state, capacitor C_{samp} is not expected to have significantly discharged over one sample interval since the 484 ns time constant is almost 10 times the sample period of Fs.

FIGURE 6. Incoming TMA RX signal in frequency domain.

FIGURE 7. RX signal after generic TMA operation – beam harmonics for phased array use created.

From the data sheet, the ADG702 has a minimum latency of 12 ns between the digital control signal changing and its analog output switching, which limits the maximum *Fs*. In practice, we have found that the minimum acceptable 'on' duration for the ADG702 is 7.9 ns.

The prototype system uses an FPGA to sequence the switches, with an internal clock running at 120 MHz and generating the TMA frame frequency *Fp* of 1 MHz (i.e., 1/*Tp*) and *Fs* of 20 MHz. The 120 MHz master clock means the FPGA file has 120 STMA control words per one *Tp* frame. There are 6 words per subsample period *Ts* frame (i.e., 1/*Fs*), hence 20 *Ts* events per one *Tp* frame. A single *Ts* sample duration event (i.e., ADG702 control bit on-time) lasts 8.33 ns and represents the maximum switching speed possible. During lab tests it was observed that switching the ADG702 faster than this leads to unreliable performance. Each FPGA control word consists of the bit pattern for the full STMA at that instant in the STMA frame- with each bit corresponding to the state of each associated STMA cell switch.

B. FREQUENCY PLANNING FOR STMA

To understand the frequency domain operation of the STMA, consider an incoming RX signal presented to the TMA cell, as represented by Fig. 6. Where required due to switch BW limitations the initial conversion down from F_c to *IF1* can be performed by a conventional mixer, as already discussed. If higher performance switches are available, then this initial down conversion stage could be removed and the STMA operate directly at F_c.

The output signal from an ideal TMA switch, such as in Fig. 1, will consist of *IF1* mixed with harmonics of the TMA switching frequency *Fp*, as illustrated in Fig. 7. The *C1p* harmonic is at *IF1* + *Fp*, *C1n* harmonic is at *IF1* – *Fp*, *C2p* harmonic is at *IF1* + 2*Fp* and *C2n* harmonic is at *IF1* – 2*Fp*.

Each resulting harmonic (*C0, C1n, C1p, C2n, C2p, …,*) will have a different phase shift due to the TMA control waveform timings. This phase shift implements the required phased array for receive array coherence at a particular wavefront angle of arrival, for that harmonic - hence creating an RX harmonic beam. The designer's task is to select which of these harmonic beams is of interest and to down convert

FIGURE 8. RX sampling spectrum of STMA showing Nyquist alias bands from subsampling.

it using the subsampler. The subsampling process uses the images that are created by the sampler operation, as represented in Fig. 8. The RF signals from the TMA placed in a high Nyquist band are thus translated down to a low IF (*IF2*) and so realize the STMA. Due to the subsampling, care must be taken to ensure unused Nyquist bands are clear of any input signals.

The important relationship between the TMA switching frequency and sampling rate will now be discussed. It is important to consider how all the generated spectral components are handled by the subsampling process, to avoid unwanted imaging and aliasing problems which may corrupt the desired harmonic beam RX signal. The resulting subsampled *IF2* signal can be predicted by (3),

$$IF2 = \left(IF1 + nF_p\right) - pF_s \tag{3}$$

where *Fs* is the sampling frequency, *Fp* is the STMA frame rate (1/*Tp*), *IF1* is the input down converted carrier frequency, *n* is the TMA harmonic beam being used to implement the array phase shift (…, –2, –1, 0, 1, 2,…) and *p* is the sampling frequency harmonic being used for subsampling. For simplicity, the input signal to subsample is assumed to be fully contained in the normal Nyquist bandwidth [0, *Fs*/2].

In the prototype RX system, we use $Fs = 20$ MHz, $Fp = 1$ MHz, $IF1 = 184.5$ MHz, $p = 9$, $n = 0$. This results in the *C0* RX beam being subsampled to 4.5 MHz, the *C1p* beam to 5.5 MHz and *C1n* beam to 3.5 MHz, the *C2n* beam is resolved at 2.5 MHz and the *C2p* beam at 6.5 MHz. Care must be taken to avoid the subsampled signals landing on system clock switching harmonics, most notably due to *Fp*. This is avoided by choice of F_c, *Fs* and *Fp* to ensure that the desired *IF2* signals all land in between harmonics of *Fp*. Corruption from aliasing is also avoided by down converting all negative and positive beams from the STMA process to *IF2*, hence the *C0* beam appearing at 4.5 MHz and not at 0 Hz. If a narrow band pass filter (BPF) was provided in between the TMA switch and a subsampler switch any unwanted TMA harmonic beams could have been removed before down conversion. However, this would require two switches with a BPF in between - which is more complex and so reduces the benefit of the proposed STMA technique. Therefore, here all the generated STMA harmonics must be handled by the subsequent RX system.

C. STMA CONTROL WAVEFORMS

The RX (or TX) beam pattern Array Factor (AF) for a conventional TMA using isotropic radiating elements can be predicted based on the time domain control waveforms controlling the RF switches [7], [34]. The AF can be calculated using (4) where *N* is the number of antenna elements,

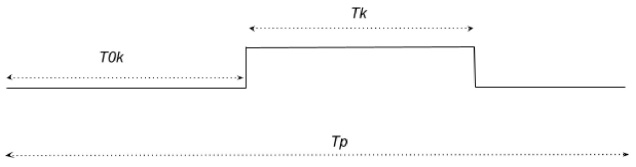

FIGURE 9. TMA switch control timings (no subsampling).

$F_n[U_k(t)]$ is the Fourier coefficient of the nth harmonic (. . . , –2, –1, 0, 1, 2,. . .) of the time domain switching waveform U on the kth antenna element.

$$\mathrm{AF}(\theta, t, n) = e^{j[\omega_c + n\omega_p]t} \sum_{k=1}^{N} F_n[U_k(t)] e^{j\varphi_k} \tag{4}$$

The time modulation of the incoming RF signal at element k can be represented as a series of Fourier coefficients, multiplied with harmonics of the switching frequency $\omega_p = (2\pi F_p)$, mixed with the carrier frequency $\omega_c = (2\pi F_c)$. The term $e^{j\varphi_k}$ is an element-specific phase shift, due to antenna element spacing and evaluated beam angle and can be expressed using (5), where d is the spacing between the elements, θ is the azimuth beam angle direction being evaluated and λ is the carrier wavelength.

$$\varphi_k = (k-1)\frac{2\pi}{\lambda} d.\sin(\theta) \tag{5}$$

The nth Fourier coefficient of the switching waveform (nth harmonic), for a particular element k, is $\mathrm{Cn}_k = F_n[U_k(t)]$ and the overall magnitude of the combined AF due to the nth harmonic is *Cn,* which can be for a positive beam steer (*C1p, C2p*) or negative beam steer (*C1n, C2n*) or boresight *C0.* The AF for a given applied switch timing set, at a given harmonic *n,* and resulting in a beam at $[\omega_c + n.\omega_p]$ is found using (6) [34], where T_k is the on duration of the element switch and T_{0k} is the delay before the switch turns on.

$$\mathrm{AF}(\theta, n) = \sum_{k=1}^{N} e^{j\varphi_k} \frac{\sin\left(n.\pi \frac{T_k}{T_p}\right)}{n.\pi} e^{-\mathrm{j}n\pi\left(2\frac{T_{0k}}{T_p} + \frac{T_k}{T_p}\right)} \tag{6}$$

The timing parameters for a conventional TMA switched element are illustrated in Fig. 9.

Therefore, in a conventional TMA, the individual switches in the RF path are turned on and off according to a required pattern to achieve a desired beam steer on a selected harmonic at an angle of interest, such as using (6). The required switch timings T_k and T_{0k} to steer a harmonic beam of interest can be calculated using the techniques described in [34].

An example of such a control pattern for an 8 element TMA steering the positive first harmonic beam (*C1p*) to +15 degrees is shown in Fig. 10(a). Another example is shown in Fig. 10(b) for a positive second harmonic beam (*C2p*) steered to +25 degrees. In a subsampling TMA, with the sampler and TMA function combined, the resulting STMA switch control pattern must now incorporate both the expected TMA element timings and also the sampling event

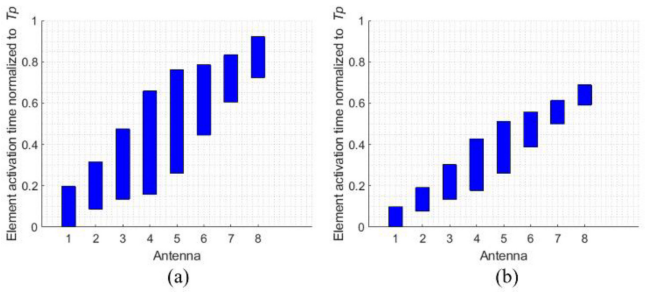

FIGURE 10. Conventional TMA antenna element timings (blue bar defines switch is on) (a): beam *C1p* steered to 15 degrees, (b): beam *C2p* steered to 25 degrees.

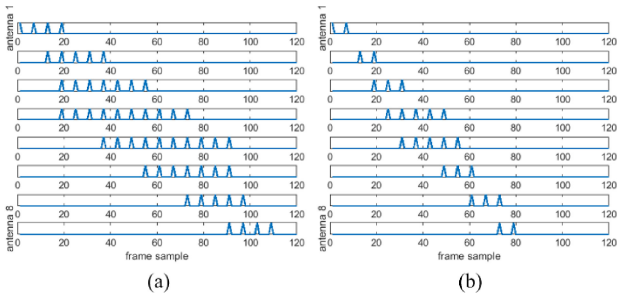

FIGURE 11. STMA antenna element switch timings (*Ts* sample instants shown) (a): beam *C1p* steered to 15 degrees, (b): beam *C2p* steered to 25 degrees.

at Fs. This is pragmatically achieved by the product of both these timing sequences. An example of this is shown for a *C1p* harmonic beam steered to +15 degrees and with a *Fs/Fp* ratio of 20 in Fig. 11(a).

In Fig. 11(b), the switch control pattern is shown for harmonic beam *C2p* steered to +25 degrees. Notice that there are fewer on events in the *C2p* harmonic pattern of Fig. 11(b) compared to Fig. 11(a). This leads to a reduction in *C2p* recovered *IF2* power compared to the *C1p* power, due to the average on time affecting the magnitude of received power as will be discussed next.

D. STMA ARRAY CONVERSION GAIN

Since the STMA incorporates a frequency conversion action, we will refer to the system gain as resolved at *IF2* relative to a known applied EIRP RF power at the antenna as the Array Conversion Gain (ACG). The subsampling action, when not using the TMA mode, has a negligible effect on the ACG when comparing the magnitude of recovered *IF2* vs *IF1*. However, when the TMA mode is also used there is a reduction in effective ACG seen on higher harmonic beams due to the limited number of sample events per STMA element within frame *Tp*. This Harmonic Level Reduction (*HLR*) factor is approximated by (7), where *C2p_tot_on* is the total number of sampling switch on events summed across all antennas when considering *C2p* beam and *C1p_tot_on* is the total number of on events summed across all antennas when considering *C1p* beam, in period *Tp*. In our implementation as seen in Fig. 11, $C1p\_tot\_on = 52$ and $C2p\_tot\_on = 25$, with (7) then predicting a 6.4 dB reduction in the *C2p*

TABLE 1. Sampler-induced harmonic beam levels relative to *C0* beam (used as *SGRF*).

C2n level relative to *C0* (dB)	*C1n* level relative to *C0* (dB)	*C1p* level relative to *C0* (dB)	*C2p* level relative to *C0* (dB)
5.1	2.2	-1.7	-3.2

received beam power compared to the *C1p* beam.

$$HLR = 10\log_{10}\left(\frac{C2p\_tot\_on}{C1p\_tot\_on}\right) \tag{7}$$

The sampler circuit used has an implicit low-pass response, due to combination of C_{samp}, R_p, $Rswitch_{ON}$ and $Rout_{opamp}$. This results in an amplitude slope as function of *IF2* frequency so that resolved RX beams with IFs below the *C0* beam frequency (4.5 MHz) are received at a higher signal level than the beams above the *C0* frequency. One solution to this frequency response slope would be a smaller *Rp* value but this would directly impact the hold performance of the sampler, which is very undesirable. Spice simulation of only the sampler circuit allows the roll off to be predicted, with resulting expected *IF2* beam levels with respect to the *C0* beam presented in Table 1.

The Sampler Gain Reduction Factor (*SGRF*) results of Table 1 are used later when validating the lab measured gains.

III. STMA HARDWARE PLATFORM

To allow the RX STMA to be evaluated in the laboratory, a hardware prototype was created, using the circuitry described in Section II. Eight ceramic monopole antennas, 2450AT43F0100 from Johanson Technology Ltd, were used to feed the RX STMA. The PCB is standard 1.6 mm thick FR4, measuring 39 cm x 30 cm. The antenna spacing is 45 mm, with TMA control waveforms designed to suit this element spacing.

Based on device data sheets, the expected STMA cell conversion gain (F_c RF input to *IF2* out, including AD8009 combiner circuit of Fig. 5) is 6.0 dB. The expected ideal ACG for eight elements is 15 dB. The STMA control waveforms are designed using the techniques of [34] for a sidelobe level of –20 dB, using Dolph-Chebyshev weightings.

The timing control signals were created in MATLAB and loaded into an Intel EK-10M50F484 FPGA development board which was then plugged directly into the back of the STMA RF PCB to sequence it. The fully built STMA PCB is shown in Fig. 12 and the detail for one STMA cell and associated RF down converting front end is shown in Fig. 13.

A. HARDWARE PLATFORM VERIFICATION

The conducted gain, from the cell antenna test port connector, was measured by lifting the antenna link resistor R17 and fitting R18 and feeding in RF F_c signals. The *IF2* output was measured for each cell in turn when operating only in *Ts* mode with no TMA pattern loaded, with results shown in Table 2. From Table 2, the *Ts* mode average conversion gain was measured to be 8.4 dB, which compares well to the theoretical line-up value of 6.0 dB based on data sheet nominal values. After including estimates of PCB routing losses and the gain of the ceramic antenna, the overall 8 element radiated ACG is expected to be 13.0 dBi as measured at *IF2* combined output. The average measured 1 dB input compression point (IP1dB) at F_c was –30 dBm, at the RF input test connectors.

The operation of the sampler circuit was also investigated. An example captured waveform of the voltage across C22

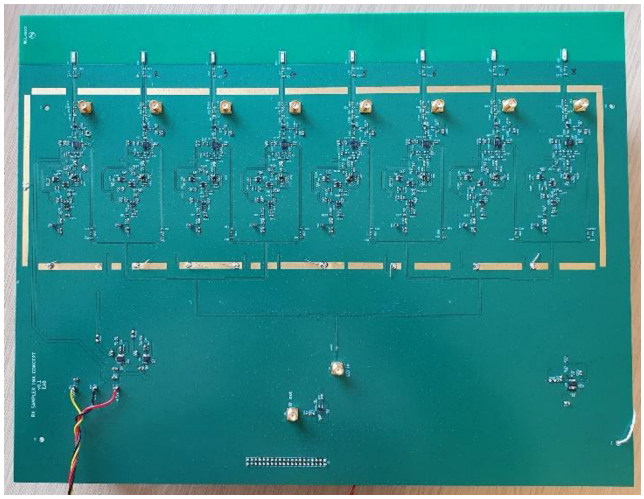

FIGURE 12. Built PCB showing 8 STMA RX cells (antennas and test connector for cell calibration visible at top, IF2 output and LO input connectors towards bottom).

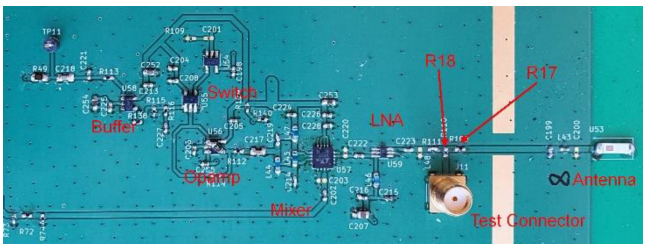

FIGURE 13. Detail of built PCB showing 1 of the 8 STMA RX cells with antenna, RF test connector used for calibration and key circuit functional blocks marked.

TABLE 2. Lab measured STMA cell conversion gains when only in subsampling mode (no TMA pattern applied).

STMA cell	Conversion gain in subsampling mode (dB)
1	8.2
2	10.3
3	8.8
4	6.1
5	8.0
6	8.9
7	8.5
8	8.4

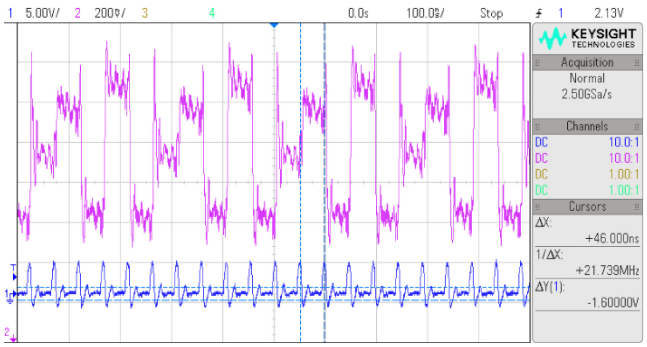

FIGURE 14. Example time domain capture of sampler waveform when processing a signal at *IF1* (upper trace showing voltage on C22 and lower trace showing *Ts* sample event).

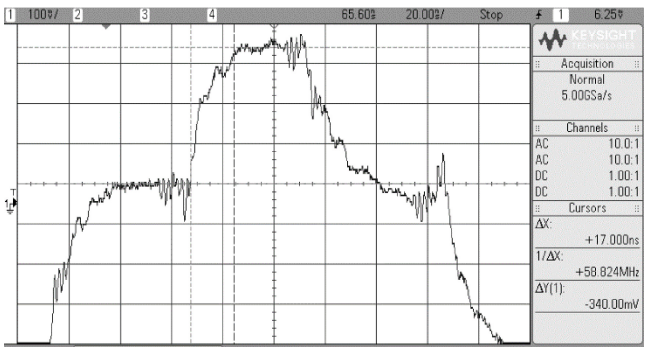

FIGURE 15. Example time domain capture of 3 cycles of *Ts* sampler capacitor C22 voltage, showing 17 ns rise and 33 ns hold times in a 50 ns sampling interval.

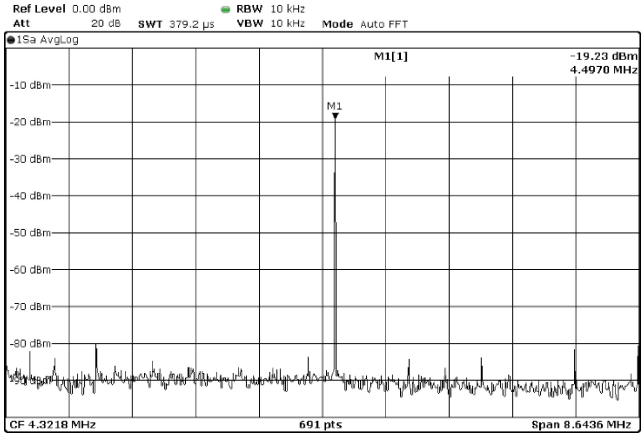

FIGURE 16. Output spectrum showing IF2 centred at 4.5 MHz for an Fc radiated test signal at 0 degrees (TMA mode disabled).

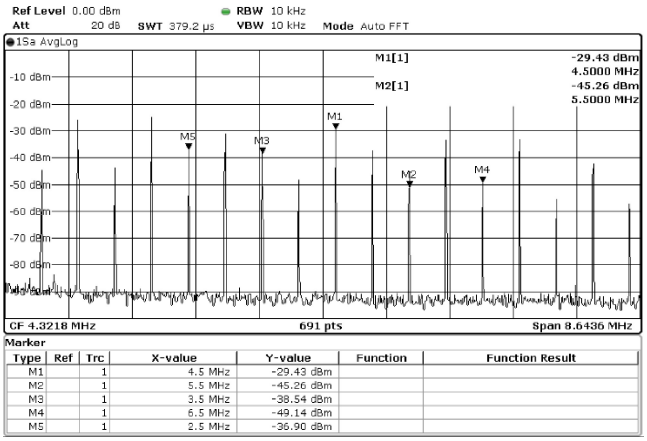

FIGURE 17. *IF2* output with *C0* centred at 4.5 MHz, for an *Fc* radiated test signal at 0 degrees (TMA mode activated, *C1p* steered to +15 degrees).

from one of the cells is shown in Fig. 14, for a sinusoidal *IF2* frequency of 4.5 MHz and *Fs* of 20 MHz. The general expected operation of the sampler can be seen, with the sampled signal changing to a new value at each sampling instant, though also with other artefacts visible.

The time domain operation was further investigated, with a zoom in view of 3 sampling events shown in Fig. 15. The peak in the centre of the plot has a rise time is 17 ns from the previously 'held' value and so the hold time appears to be 33 ns in the 50 ns sample period. Though this may seem worse than the circa 8–12 ns switchover latency expected from Section II, note that the sampled signal is sinusoidal so will not be a steady value during the finite and non-zero period the sampling switch is on. The longer slope effect is also suspected to be due to non-ideal switching within the ADG702. However, in Fig. 14 and Fig. 15 the sampler is seen to be holding the value once charged and the switch turned off. Hence, the circuit is an acceptable approximation of a sampler for the purposes of the STMA demonstrator, though it does affect overall performance as is seen later.

The non-ideal time domain nature of the sampled waveform is clear. However, an example of the spectrum seen at the *IF2* combined output when receiving a radiated signal at *Fc* with TMA mode disabled and subsampling is shown in Fig. 16.

The signal was captured using a Rohde & Schwarz FSV40-N Spectrum Analyser and suggests that the subsampler, though not using ideal waveforms, is functional, usable and gives a good signal at *IF2*.

When the TMA mode is enabled, the output spectrum at *IF2* contains additional components, but the desired output is still present, centered at 4.5 MHz for the *C0* beam, along with expected components at *C1p, C1n, C2p, C2n*, etc, as shown in Fig. 17. Harmonics of *Fp* are also seen to be present. Care must be taken in selecting the IF frequencies and switching frequencies to ensure images and spurious clock harmonics do not land on the desired beam IFs. Fig. 18 shows the output at *IF2* when no signal is being received (only noise and internally generated *Fp* switching harmonics are seen).

The Signal to Noise and Distortion Ratio (SNDR) was measured at the IF output of the STMA with an input signal at IP1dB. In sampling mode, the SNDR was measured to be 61 dB for a single cell (10 kHz measurement BW). The SNDR for the full array operating in STMA mode and processing a radiated RX signal was measured to be 69 dB.

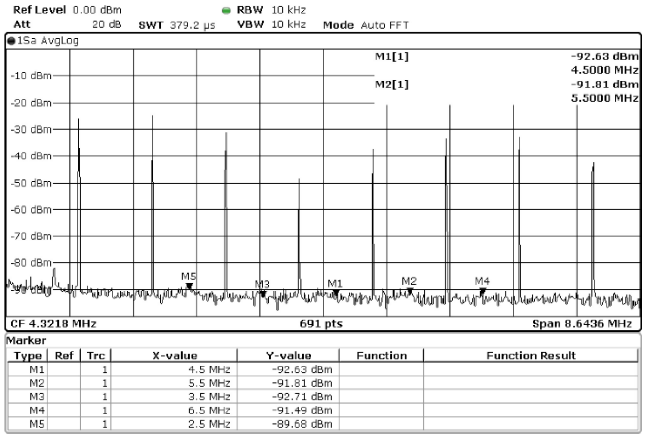

FIGURE 18. *IF2* output with *C0* centred at 4.5 MHz, RF radiated source beam off, *C1p* steered to +15 degrees (only RF noise and spurious clock signals present).

This improvement in SNDR due to TMA array operation has also been observed and predicted by others [46].

The mutual coupling between adjacent antennas was measured to be –13 dB. Between second adjacent antennas the mutual coupling was –20 dB. However, improvements to mutual coupling may be possible with a patch array.

IV. CHAMBER ARRAY CONVERSION GAIN & PATTERN MEASUREMENTS

The STMA system was evaluated in The University of Sheffield's Communication Research Group's anechoic chamber. Prior to testing, the chamber background noise level in the band was checked and found to be sufficiently low to not cause interference. The measurement system included a Rohde & Schwarz FSV40-N Spectrum Analyser and AEL H-1498 measurement horn antenna with gain of 6 dBi at 2.4 GHz. The LO signal generator for the down conversion mixers was a Keysight E4436B set to 2.24 GHz. The RF signal generator providing the wanted radiated RF signal at F_c to receive was a Keysight E4437B set to 2.4245GHz. The STMA test system setup is shown in Fig. 19(a) and the STMA PCB being tested is shown in Fig. 19(b). The test horn antennas are on an arch that allows them to be positioned as required and the STMA PCB is in the centre of the axis of rotation. The *IF2* output signals were measured using the Rohde & Schwarz FSV40-N spectrum analyser with 10 kHz resolution BW.

Radiated STMA ACGs are calculated and then reported in dBi, from the signals resolved at the subsampled *IF2* centred on 4.5 MHz for *C0*. The measured RF powers were converted to STMA ACGs from knowledge of the applied TX RF power, test horn antenna gain, distance between test horn antenna and STMA PCB (converted to an equivalent free space path loss) following the technique used in [34].

A. STEERED FIRST HARMONIC BEAM (C1P, C1N)

The theoretically expected ACG is calculated based on the initial measured conducted conversion gain from Section III

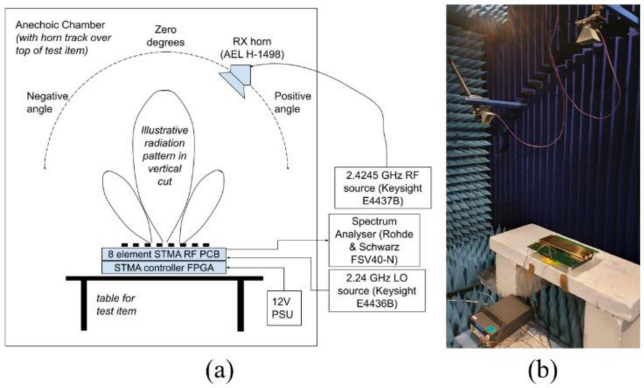

FIGURE 19. Laboratory radiated pattern measurement: (a) test system set-up, (b) example measurement.

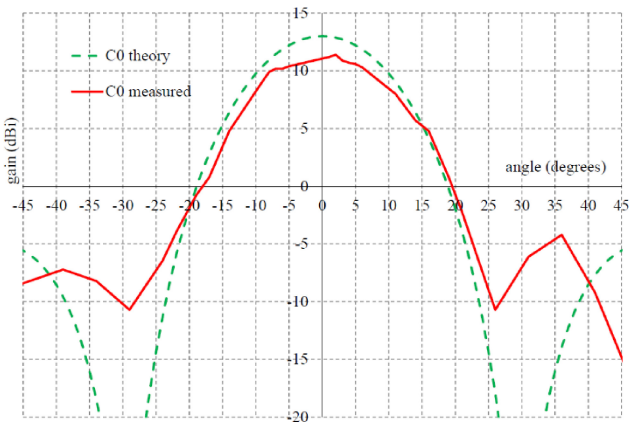

FIGURE 20. *C0* beam ACG for *C1p* steered to +15 degrees.

and its resulting expected ACG of 13.0 dBi. However, this ideal ACG must now also include effects from the AF, the sampler low pass slope (i.e., *SGRF*) and pulse losses due to chosen harmonic (i.e., *HLR*), as described in Section II. Thus, the overall expected radiated *ACG* as a function of harmonic beam and wavefront angle is found using (8), where *beam* is the harmonic beam being assessed ($n = -2$ for *C2n*, $n = -1$ for *C1n*, $n = 0$ for *C0*, $n = 1$ for *C1p*, $n = 2$ for *C2p*). *SGRF* is zero for the *C0* beam and *HLR* is only applied if *C2p* or *C2n* beams are being assessed.

$$\begin{aligned} ACGexpected(beam, \theta) = {} & 13.0 + SGRF(beam) \\ & + HLR_{(only\ if\ C2p,\ C2n\ beam)} \\ & + 20\log_{10}(AF(\theta, n)) \end{aligned} \tag{8}$$

Tests were first performed with the STMA timings set to receive a radiated beam at +15 degrees on the *C1p* harmonic, with results shown in Fig. 20 for the *C0* beam and Fig. 21 for the *C1p* beam, all compared to (8). The system was then configured to receive a *C1p* beam at –15 degrees, with results show in Fig. 22, again compared to (8).

As discussed earlier, the sampler has an LPF response, and this means that the negative harmonic beams (*C1n*, *C2n*) have a higher *IF2* output than the corresponding positive

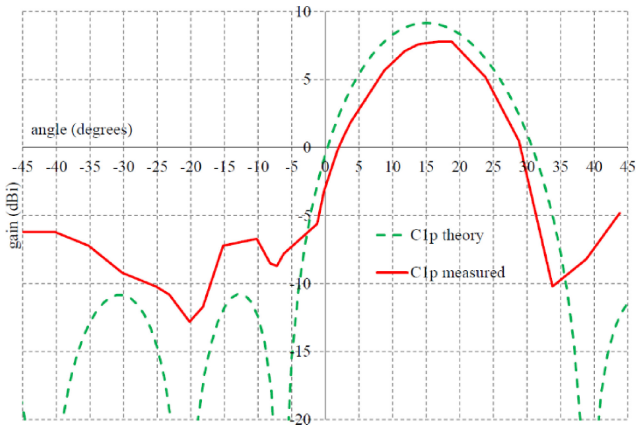

FIGURE 21. *C1p* beam ACG for *C1p* steered to +15 degrees.

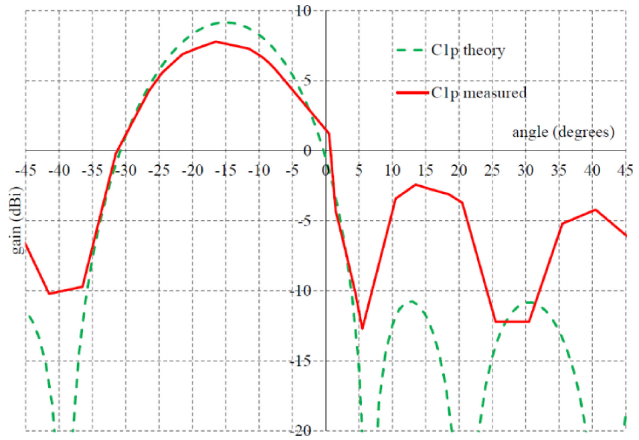

FIGURE 22. *C1p* beam ACG for *C1p* steered to –15 degrees.

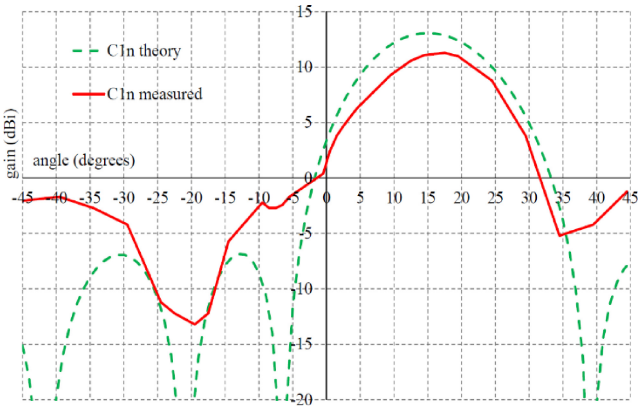

FIGURE 23. *C1n* beam ACG for *C1n* steered to +15 degrees.

steered harmonic beams (*C1p*, *C2p*). This effect can be seen in Fig. 23 where the *C1n* beam was steered to +15 degrees and shows a 3.5 dB higher gain than the *C1p* beam steered to +15 degrees as seen in Fig. 21. This level difference agrees well with the 3.9 dB predicted for *C1p*-*C1n* level delta predicted in Table 1.

Overall, for *C1p* and *C1n*, the measured gain patterns for the main lobes agree well with theoretical expectation and

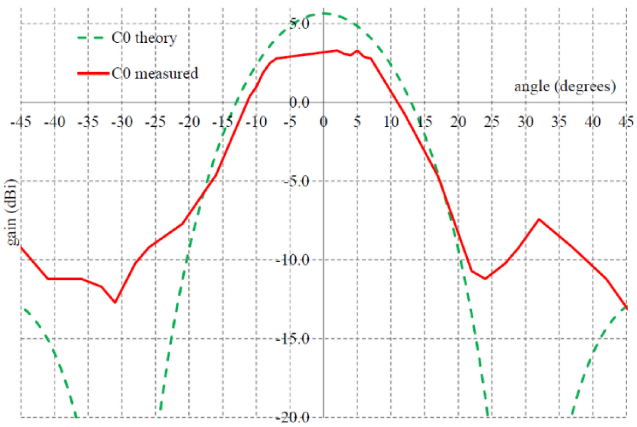

FIGURE 24. *C0* beam ACG for *C2p* steered to +25 degrees.

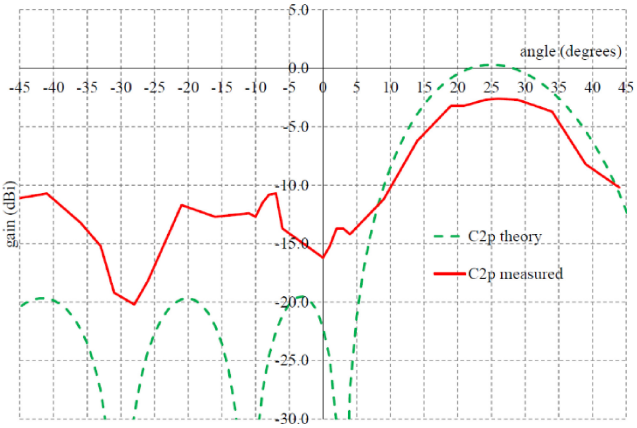

FIGURE 25. *C2p* beam ACG for *C2p* steered to +25 degrees.

show good conversion gain, though the sidelobe response is degraded compared to theoretical expectation.

B. STEERED SECOND HARMONIC BEAM (C2P, C2N)

Tests were then performed with the STMA timings set to receive a *C2p* beam at +25 degrees, with results compared to (8) in Fig. 24 for the *C0* beam and Fig. 25 for the *C2p* beam.

The results for the *C2p* beam steered to –25 degrees are shown in Fig. 26. The resulting gain when *C2n* beam was steered to +25 degrees is shown in Fig. 27, showing a 7.9 dB higher gain is obtained compared to Fig. 25, due to the LPF response of the sampler as discussed earlier. This level difference agrees well with the 8.3 dB predicted for *C2p*-*C2n* level delta predicted in Table 1.

Overall, for *C2p* and *C2n* RX beams, the measured gain patterns for the main lobes agree well with theoretical expectation and show usable ACG, particularly on the negative harmonic beams, though the sidelobe response is degraded compared to theoretical prediction.

V. DISCUSSION

Though the STMA is showing generally correct operation, analysis has been conducted to investigate possible reasons

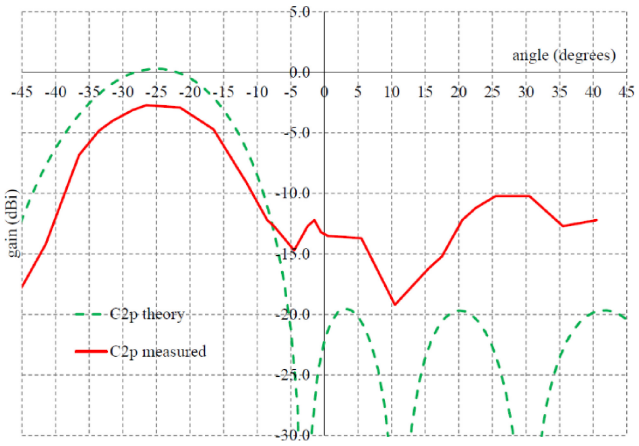

FIGURE 26. *C2p* beam ACG for *C2p* steered to –25 degrees.

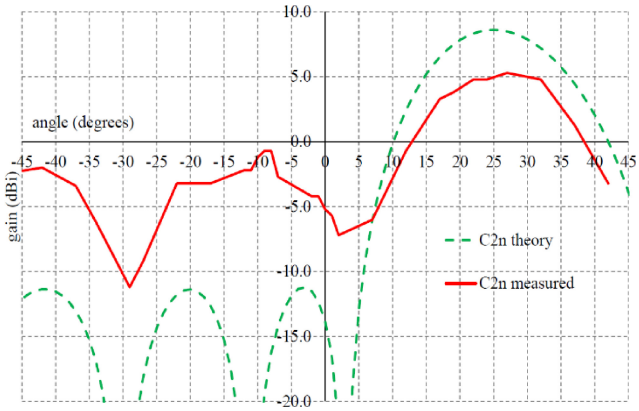

FIGURE 27. *C2n beam ACG for C2n steered to +25 degrees.*

for the observed degradation in sidelobe performance. As an example, the observed sidelobe levels for the first harmonic beams are circa –10 dB to –15 dB, instead of the –20 dB as designed. From earlier, it is known that the ADG702 based sampler has a rise time of approximately 17 ns in a sampling period of 50 ns (i.e., 34% of *Tp*). An investigation using techniques from [34] to investigate the dependency of sidelobe levels on rise time (*Tr*) and fall time (*Tf*) has shown that a 34% *Tr* (with 0.1% *Tf*) on a 1 MHz *Fp* leads to an increase in sidelobe levels to –12 dBc from a design target level of –20 dBc for the first harmonic sidelobes: similar to what was measured. From these same prediction simulations, a 2.5% *Tr* would lead to a 1 dB reduction in sidelobe level performance from the design target. This shows that the performance of the sampler switch is very important in sidelobe control and is likely a significant contributor to the sidelobe results measured in the laboratory tests. It is also possible that the sidelobe degradation is affected by a smaller amount due to a) radiated leakage directly onto the PCB circuits from imperfect PCB screening enclosures and b) from the –13 dB to –20 dB measured mutual coupling between antenna elements.

However, the ability to steer the desired incoming RF receive beam at F_c and resolve it at the subsampled *IF2* is demonstrated, validating the STMA technique and illustrating what can be achieved with imperfect hardware. Also, the main steered ACG lobe generally matches theoretical expectations well. The measured peak ACGs are 11.4 dBi for the *C0* beam, 7.8 dBi for the *C1p* beam, 11.3 dBi for the *C1n* beam, –2.6 dBi for the *C2p* beam and 5.3 dBi for the *C2n* beam.

Achieved ACG is lower for second harmonic beams, as anticipated and also seen in other works [34], however is still useful. Also, as predicted, we note that negative harmonic beam ACGs are higher than positive harmonic beams, due to sampler circuit LPF response. This suggests that a practical system could benefit from using only the negative beams for steering, to minimise the impact of the SGRF. Alternatively, the *C0* beam also gives good ACG and sidelobe performance and so could be used for a non-steerable STMA array.

One potential issue seen is the presence of the *Fp* harmonics in the output *IF2* spectrum, requiring careful frequency planning to avoid them corrupting the wanted signals. The *Fp* harmonic components are due to the periodic switching of the *IF1* signal which has a background DC component. It may be possible to reduce the magnitude of the *Fp* harmonics seen by use of differential switching techniques in the sampler, though this would increase complexity.

Cracking and subsequent failing of some ceramic capacitors in the RF signal chain was also experienced during tests and required occasional replacements. This failure mechanism is a well-known issue in industry and care was taken during tests to ensure results were always obtained from a fully functional system.

Overall, we propose that the STMA is a novel enhancement of a TMA, that could help reduce the hardware complexity of a conventional phased array receiver system by allowing the removal of a mixer stage prior to the ADC. Such a mixer stage would often usually be required to create an IF signal within the ADC passband. The use of the STMA concept also allows reduction of the ADC sample rate otherwise needed to directly digitize from a high IF (in the first Nyquist band), if subsampling of the ADC input had not been used. Our practical work verifies the expected operation of the STMA.

In our demonstration system we were forced to use down conversion mixers prior to the STMA cells, due to RF BW limitations of the sampler switch. If a switch was available that could pass carrier signals at *Fc* and switch at the desired *Fs,* then this mixer stage would not have been required.

However, the strategy of a mixer-first STMA could be useful for mmWave systems, where suitable sampler switches are not yet be viable but a phased array is needed.

Table 3 compares the performance of the STMA concept demonstrator to relevant published works in receiver DBFs and ABFs, operating with carriers below 6 GHz. Parameters compared include array Side Lobe Level (SLL), Effective

TABLE 3. Comparison of STMA systems to prior works at sub 6 GHz.

	[55]	[56]	[54]	**This work**
Technique	IF sampling DBF	Time delay DBF	Microwave sampling	STMA
Carrier (MHz)	260	1000	5800	2420
RF BW (MHz)	20	100	6.49	1
Elements	8	16	4	8
ACG (dBi)	-	-	-	13
Cell Conversion Gain (dB)	-	-	Loss (due to pin diodes)	8.4
Cell IP1dB (dBm)	-	-	-	-30
SLL (dB)	-14 (single beam)	-13 (-30 degree steer)	-15.5 (SLL & scanning control)	-15 (*C0*) -10 .. -15 (*C1p, C1n*)
Sampler Clock	1040 MHz	4 GHz	6.49 MHz	20 MHz *Fs*, 1 MHz *Fp* (120 MHz FPGA)
Array SNDR (dB)	63.3	60	-	69 (10 kHz BW)
Array output	Digital	Digital	IF, 5.79351 GHz (1st lower harmonic)	IF, 4.5 MHz
Max. scan angle reported (degrees)	60	90	-50	+ / - 15 (*C1p*) +/- 25 (*C2p*)
DC power	124mW (65 nm CMOS)	453 mW (40 nm CMOS)	8 – 14 mA per diode	978 mW / cell
Phase Resolution	240 steps using 12 bits (7.9 ENCB)	1 degree (10 bits)	1.4 degrees (8 bits)	6.9 ENCB (FPGA timing)
Amplitude Resolution	-	-	12 bits	6.9 ENCB (FPGA timing)

Number of Control Bits (ENCB) and input 1 dB compression point (IP1dB). Although our demonstration system is primarily intended to illustrate the STMA concept (using commercially available generic components with associated power efficiency issues), it is still clear from Table 3 that the STMA performance for gain, SLL and SNDR is competitive. The low RF BW is due to FPGA maximum clocking frequency issues and the number of TMA pattern words used. This could be improved with different baseband hardware.

The simple (1 bit per cell) control interface and low IF output are key advantages. The STMA is the only work considered that has a low frequency IF output (4.5 MHz) from a high carrier frequency, which significantly simplifies the requirements for subsequent digitization.

The nearest conceptual work to ours is [54] but this does not subsample, so the down conversion is due to the switching harmonics. The harmonics in [54] will rapidly reduce in magnitude as they extend further from the carrier and so requires extremely high clocking rates to obtain a resultant low IF using only the first or second harmonic. Subsampling does not suffer from this effect.

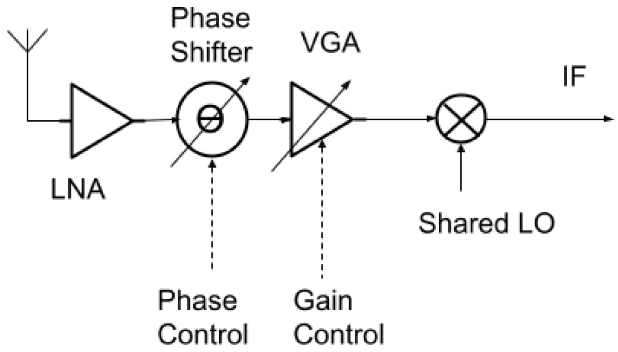

FIGURE 28. Conventional ABF cell (combination of cells can be before or after mixer).

TABLE 4. Cost and power model examples at 2.4 GHz using commercial parts (costings are based on current manufacturers' pricing for 500 off).

Function	Example part	Usage	Item cost (USD, 500 off)	Item power (mW)
LNA	HMC374	ABF + STMA	3.66	247.5
Phase Shifter	HMC647A (6 bits)	ABF	84.5	75
VGA	HMC742A (6 bits)	ABF	13.75	650
Mixer	LT5527	ABF	8.51	390
Buffer	AD8009	STMA	2.45	70
Sampler	ADG702	STMA	1.21	0.005
Buffer	BUF602	STMA	0.936	270

A. COST AND POWER CONSIDERATIONS

We will now consider the STMA cost and power, compared to an ABF in example beamformer implementations. As a first example, consider a 2.4 GHz phased array ABF with cell as shown in Fig. 28 and compare this to the STMA optimal approach (no initial down conversion mixer) of Fig. 2. For the sake of the illustration, we will ignore the upper frequency limits of the ADG702 switch and so assume the initial mixer of Fig. 3 is not required. The cost and power consumption for each commercial part used in the prototype 2.4 GHz system and their applicability to either the ABF or STMA are listed in Table 4, with a possible VGA and phase shifter.

From Table 4, one cell of the ABF would consume 1021 mW and cost 103 USD. This assumes signal combination from all the cell branches occurs at the 2.4 GHz carrier and so only one down conversion mixer is required. In comparison, a single cell of the STMA would require 587 mW and cost 8.3 USD, representing a saving of 95 USD (92%) and 434 mW (43%) compared to the conventional ABF example. Though crude, the above example shows cost and power savings for a given semiconductor technology can be expected when using the STMA approach. It is also worth

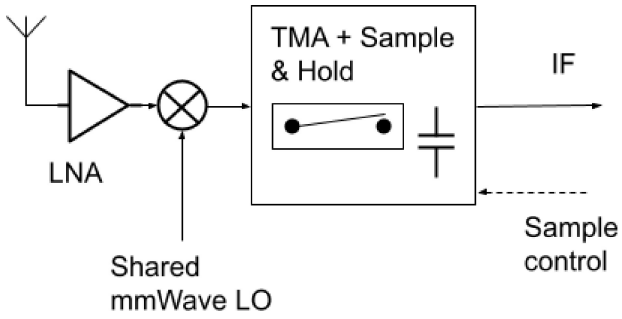

FIGURE 29. Prototype mmWave STMA cell with mixer-first down conversion to intermediate IF due to limited switch RF BW.

noting that the example phase shifter and VGA parts require 12 control bits in total, compared to the single digital bit for the STMA.

We now go on to consider the potential advantage of using the STMA at 28 GHz using recent published works to help illustrate. To realize a conventional ABF at 28 GHz would require a suitable phase shifter, for example [39] which requires 6 control bits, is passive and requires 0.53 mm^2 of wafer material. A VGA is also required, such as [40] which requires analogue control lines, draws 23 mW and consumes 0.103 mm^2 of wafer die. Alternatively, a combined phase shifter and VGA, such as [57] requiring both analog control and 6 digital bits whilst drawing 23 mW could be considered. In contrast, the STMA would likely require a mmWave to microwave down converting mixer, such as [58] requiring 6.4 mW and 0.52 mm^2 of die, which could be followed by a suitable 'cold-FET' zero-bias switch to implement the STMA sampler function, as illustrated in Fig. 29. If such a sampler switch were available and capable of sufficient switching speed, then a power saving of circa 16.6 mW (72%) and area saving of circa 18% could be obtained, (ignoring issues relating to wafer material differences). It would be more cost effective to have the sample-hold capacitor off-chip due to its large physical area. Power efficiency savings are increasingly important for large arrays, which are required for mmWave systems.

If the STMA mixer-first approach were not required for mmWave operation, then the wafer savings and DC power savings would be significantly greater, perhaps requiring only a few square microns of semiconductor material for the sampling switch and an off-chip sample-hold capacitor. However, significant research work is now needed in creating fast switches for use in a STMA, possibly via tail current switched amplifiers [46].

The STMA single digital control line to control the down conversion and beam steering is an important advantage. As illustrated above, conventional beamformers require multiple control lines for the phase shifter and VGA. For large arrays, arranging and routing sufficient control lines can be difficult.

VI. CONCLUSION

An STMA system which directly incorporates subsampling within a receive TMA is discussed and demonstrated. The system shows STMA receive array beams can be steered at the carrier F_c and resolved at the subsampled IF2, as predicted.

The concept could be applied to any frequency band, though the design of the sampling switch is a critical feature which dictates the maximum design frequencies and side-lobe performance. The STMA concept could be applied to carriers above the BW of the sampling switch by use of a simple down conversion mixer stage before the STMA cell, as demonstrated in our work. Such concepts could allow a pragmatic application of the STMA to mmWave or higher bands.

Potential power and cost savings for the STMA are presented using examples. The STMA concepts could also be applied to a TX system, with appropriate modifications to use the up-sampled Nyquist images from a DAC or similar.

REFERENCES

[1] C. Casetti, "The challenges of universal broadband connectivity [mobile radio]," *IEEE Veh. Technol. Mag.*, vol. 17, no. 3, pp. 5–11, Sep. 2022, doi: 10.1109/mvt.2022.3176414.

[2] W. Hong et al., "The role of millimeter-wave technologies in 5G/6G wireless communications," *IEEE J. Microw.*, vol. 1, no. 1, pp. 101–122, Jan. 2021, doi: 10.1109/jmw.2020.3035541.

[3] R. Chataut and R. Akl, "Massive MIMO systems for 5G and beyond networks—Overview, recent trends, challenges, and future research direction," *Sensors*, vol. 20, no. 10, p. 2753, May 2020, doi: 10.3390/s20102753.

[4] W. H. Kummer, A. T. Villeneuve, T. S. Fong, and F. G. Terrio, "Ultra-low sidelobes from time-modulated arrays," *IEEE Trans. Antennas Propag.*, vol. AP-11, no. 6, pp. 633–639, Nov. 1963, doi: 10.1109/TAP.1963.1138102.

[5] Y. Tong and A. Tennant, "Simultaneous control of sidelobe level and harmonic beam steering in time-modulated linear arrays," *Electron. Lett.*, vol. 46, no. 3, pp. 200–202, Feb. 2010, doi: 10.1049/el.2010.2629.

[6] W.-Q. Wang, H. C. So, and A. Farina, "An overview on time/frequency modulated array processing," *IEEE J. Sel. Topics Signal Process.*, vol. 11, no. 2, pp. 228–246, Mar. 2017, doi: 10.1109/JSTSP.2016.2627182.

[7] G. Li, S. Yang, Y. Chen, and Z. Nie, "A novel beam scanning technique in time modulated linear arrays," in *IEEE Antennas Propag. Soc. AP-S Int. Symp. Dig.*, North Charleston, SC, USA, 2009, pp. 1–4, doi: 10.1109/APS.2009.5171609.

[8] P. Rocca, G. Oliveri, R. J. Mailloux, and A. Massa, "Unconventional phased array architectures and design methodologies—A review," *Proc. IEEE*, vol. 104, no. 3, pp. 544–560, Mar. 2016, doi: 10.1109/JPROC.2015.2512389.

[9] Y. Tong and A. Tennant, "A two-channel time modulated linear array with adaptive beamforming," *IEEE Trans. Antennas Propag.*, vol. 60, no. 1, pp. 141–147, Jan. 2012, doi: 10.1109/TAP.2011.2167936.

[10] T. E. Bekele et al., "Advances on time-modulated arrays for cognitive radio," in *Proc. 7th Eur. Conf. Antennas Propag. (EUCAP)*, Gothenburg, Sweden, 2013, pp. 344–346.

[11] L. Poli, P. Rocca, G. Oliveri, and A. Massa, "Harmonic beamforming in time-modulated linear arrays," *IEEE Trans. Antennas Propag.*, vol. 59, no. 7, pp. 2538–2545, Jul. 2011, doi: 10.1109/TAP.2011.2152323.

[12] R. Maneiro-Catoira, J. C. Brégains, J. A. García-Naya, L. Castedo, P. Rocca, and L. Poli, "Performance analysis of time-modulated arrays for the angle diversity reception of digital linear modulated signals," *IEEE J. Sel. Topics Signal Process.*, vol. 11, no. 2, pp. 247–258, Mar. 2017, doi: 10.1109/JSTSP.2016.2609852.

[13] M. H. Mazaheri, M. Fakharzadeh, M. Akbari, and S. Safavi-Naeini, "A time modulated array with polarization diversity capability," *IEEE Access*, vol. 9, pp. 53735–53744, 2021, doi: 10.1109/ACCESS.2021.3070492.

[14] W. C. Barott and S. Fucharoen, "Experimental time-modulated beamformer for interference mitigation in a radio spectrometer," *IEEE J. Sel. Topics Signal Process.*, vol. 11, no. 2, pp. 271–281, Mar. 2017, doi: 10.1109/JSTSP.2016.2615268.

[15] L. Poli, P. Rocca, G. Oliveri, and A. Massa, "Adaptive nulling in time-modulated linear arrays with minimum power losses," *IET Microwaves Antennas Propag.*, vol. 5, no. 2, pp. 157–166, Jan. 2011, doi: 10.1049/iet-map.2010.0015.

[16] G. Bogdan, M. Jarzynka, and Y. Yashchyshyn, "Experimental study of signal reception by means of time-modulated antenna array," in *Proc. 21st Int. Conf. Microwave Radar Wireless Commun. (MIKON)*, Krakow, Poland, 2016, pp. 1–4, doi: 10.1109/MIKON.2016.7492030.

[17] G. Bogdan, Y. Yashchyshyn, and M. Jarzynka, "Time-modulated antenna array with lossless switching network," *IEEE Antennas Wireless Propag. Lett.*, vol. 15, pp. 1827–1830, 2016, doi: 10.1109/LAWP.2016.2538463.

[18] J. Chen, R. Jin, H. Fan, J. Geng, X. Liang, and C. He, "Wideband direction-finding based on time-modulated antenna array," in *Proc. Asia–Pac. Conf. Antennas Propag. (APCAP)*, Bali, Indonesia, 2015, pp. 48–49, doi: 10.1109/APCAP.2015.7374266.

[19] A. O'Donnell, W. Clark, J. Ernst, and R. McGwier, "Analysis of modulated signals for direction finding using time modulated arrays," in *Proc. IEEE Radar Conf. (RadarConf)*, Philadelphia, PA, USA, 2016, pp. 1–5, doi: 10.1109/RADAR.2016.7485111.

[20] D. Ni, S. Yang, Y. Chen, and J. Guo, "A study on the application of subarrayed time-modulated arrays to MIMO radar," *IEEE Antennas Wireless Propag. Lett.*, vol. 16, pp. 1171–1174, 2016, doi: 10.1109/LAWP.2016.2626478.

[21] G. Li, S. Yang, and Z. Nie, "A study on the application of time modulated antenna arrays to airborne pulsed doppler radar," *IEEE Trans. Antennas Propag.*, vol. 57, no. 5, pp. 1579–1583, May 2009, doi: 10.1109/TAP.2009.2016788.

[22] J. Euziere, R. Guinvarc'h, M. Lesturgie, B. Uguen, and R. Gillard, "Dual function radar communication time-modulated array," in *Proc. Int. Radar Conf.*, Lille, France, 2014, pp. 1–4, doi: 10.1109/RADAR.2014.7060416.

[23] J. Euziere, R. Guinvarc'h, I. Hinostroza, B. Uguen, and R. Gillard, "Time modulated array for dual function radar and communication," in *Proc. IEEE Int. Symp. Antennas Propag. USNC/URSI Nat. Radio Sci. Meeting*, Vancouver, BC, Canada, 2015, pp. 806–807, doi: 10.1109/APS.2015.7304790.

[24] J. Euzière, R. Guinvarc'h, I. Hinostroza, B. Uguen, and R. Gillard, "Optimizing communication in TMA for radar," in *Proc. IEEE Antennas Propag. Soc. Int. Symp. (APSURSI)*, Fajardo, PR, USA, 2016, pp. 705–706, doi: 10.1109/APS.2016.7696061.

[25] C. Shan, J. Shi, Y. Ma, X. Sha, Y. Liu, and H. Zhao, "Power loss suppression for time-modulated arrays in radar-communication integration," *IEEE J. Sel. Topics Signal Process.*, vol. 15, no. 6, pp. 1365–1377, Nov. 2021, doi: 10.1109/JSTSP.2021.3118896.

[26] Y. Wang and A. Tennant, "Experimental time-modulated reflector array," *IEEE Trans. Antennas Propag.*, vol. 62, no. 12, pp. 6533–6536, Dec. 2014, doi: 10.1109/TAP.2014.2362129.

[27] X. Cao, Q. Chen, T. Tanaka, M. Kozai, and H. Minami, "A 1-bit time-modulated reflectarray for reconfigurable intelligent surface applications," *IEEE Trans. Antennas Propag.*, vol. 71, no. 3, pp. 2396–2408, Mar. 2023, doi: 10.1109/TAP.2022.3233659.

[28] A. Reyna, L. I. Balderas, and M. A. Panduro, "Time-modulated antenna arrays for circularly polarized shaped beam patterns," *IEEE Antennas Wireless Propag. Lett.*, vol. 16, pp. 1537–1540, 2017, doi: 10.1109/LAWP.2017.2647900.

[29] G. Bogdan, P. Bajurko, and Y. Yashchyshyn, "Time-modulated antenna array with dual-circular polarization," *IEEE Antennas Wireless Propag. Lett.*, vol. 19, no. 11, pp. 1872–1875, Nov. 2020, doi: 10.1109/LAWP.2020.2999643.

[30] A. Tennant and B. Allen, "Generation of OAM radio waves using circular time-switched array antenna," *Electron. Lett.*, vol. 48, no. 21, pp. 1365–1366, Oct. 2012, doi: 10.1049/el.2012.2664.

[31] G. Bogdan, K. Godziszewski, and Y. Yashchyshyn, "Time-modulated antenna array for real-time adaptation in wideband wireless systems—Part II: Adaptation study," *IEEE Trans. Antennas Propag.*, vol. 68, no. 10, pp. 6973–6981, Oct. 2020, doi: 10.1109/TAP.2020.3008633.

[32] Q. Chen, J.-D. Zhang, W. Wu, and D.-G. Fang, "Enhanced single-sideband time-modulated phased array with lower sideband level and loss," *IEEE Trans. Antennas Propag.*, vol. 68, no. 1, pp. 275–286, Jan. 2020, doi: 10.1109/TAP.2019.2938711.

[33] Y. Ma, C. Miao, Y.-H. Li, and W. Wu, "Harmonic beamforming based on modified single-sideband time modulated phased array and its enhanced version," *IEEE Access*, vol. 9, pp. 57819–57828, 2021, doi: 10.1109/ACCESS.2021.3072777.

[34] E. A. Ball and A. Tennant, "A technique to control the harmonic levels in time-modulated antenna arrays—Theoretical concept and hardware verification platform," *IEEE Trans. Antennas Propag.*, vol. 68, no. 7, pp. 5375–5386, Jul. 2020, doi: 10.1109/TAP.2020.2978894.

[35] X. Lu, S. Venkatesh, B. Tang, and K. Sengupta, "Space–time modulated 71-to-76GHz mm-Wave transmitter array for physically secure directional wireless links," in *Proc. IEEE Int. Solid-State Circuits Conf. (ISSCC)*, San Francisco, CA, USA, 2020, pp. 86–88, doi: 10.1109/ISSCC19947.2020.9062929.

[36] O. Gassab, A. Azrar, A. Dahimene, and S. Bouguerra, "Efficient mathematical method to suppress sidelobes and sidebands in time-modulated linear arrays," *IEEE Antennas Wireless Propag. Lett.*, vol. 18, no. 5, pp. 836–840, May 2019, doi: 10.1109/LAWP.2019.2903200.

[37] G. Bogdan, K. Godziszewski, and Y. Yashchyshyn, "Time-modulated antenna array with beam-steering for low-power wide-area network receivers," *IEEE Antennas Wireless Propag Lett.*, vol. 19, no. 11, pp. 1876–1880, Nov. 2020, doi: 10.1109/LAWP.2020.3007925.

[38] N. Singhal and S. M. R. Hasan, "Review and comparison of different limited scan phased array antenna architectures," *Int. J. Circuit Theory Appl.*, vol. 49, no. 10, pp. 3111–3130, Oct. 2021, doi: 10.1002/cta.3118.

[39] M. Wang, F. Ullah, X. Wang, Y. Xiao, and Y. Liu, "A 25-31 GHz 6-bit switch-type phase shifter in 0.13um SOI CMOS process for 5G mmWave phased array communications," in *Proc. 14th IEEE Int. Conf. Solid-State Integr. Circuit Technol. (ICSICT)*, Qingdao, China, 2018, pp. 1–3, doi: 10.1109/ICSICT.2018.8565766.

[40] J. Park and S. Hong, "Wideband bidirectional variable gain amplifier for 5G communication," *IEEE Microw. Wireless Technol. Lett.*, vol. 33, no. 6, pp. 691–694, Jun. 2023, doi: 10.1109/lmwt.2023.3244715.

[41] P. Guan et al., "A 33.5-37.5 GHz four-element phased-array transceiver front-end with hybrid architecture phase shifters and gain controllers," *IEEE Trans. Microw. Theory Techn.*, early access, Mar. 3, 2023, doi: 10.1109/TMTT.2023.3248175.

[42] C.-N. Chen et al., "36–40 GHz Tx/Rx beamformers for 5G mm-Wave phased-array," in *Proc. Asia–Pac. Microwave Conf. (APMC)*, Kyoto, Japan, 2018, pp. 756–758, doi: 10.23919/APMC.2018.8617146.

[43] W. Lv et al., "A 24-27GHz phased array transceiver with 6 bit phase shifter and 31.5dB gain control for 5G communication in 65nm CMOS," in *Proc. IEEE Int. Conf. Integr. Circuits Technol. Appl. (ICTA)*, Nanjing, China, 2020, pp. 23–24, doi: 10.1109/ICTA50426.2020.9331999.

[44] T. Kanar, S. Zihir, and N. Yanduru, "Ultra-compact and modular 5G phased-array 4-channel beamformer front-ends with <2° RMS phase error," in *Proc. IEEE/MTT-S Int. Microwave Symp. (IMS)*, Philadelphia, PA, USA, 2018, pp. 1327–1329, doi: 10.1109/MWSYM.2018.8439596.

[45] R. Lu, C. Weston, D. Weyer, F. Buhler, D. Lambalot, and M. P. Flynn, "A 16-element fully integrated 28-GHz digital RX beamforming receiver," *IEEE J. Solid-State Circuits*, vol. 56, no. 5, pp. 1374–1386, May 2021, doi: 10.1109/JSSC.2021.3067504.

[46] T.-Y. Huang, B. Lin, N. S. Mannem, B. Abdelaziz, and H. Wang, "A time-modulated concurrent steerable multibeam MIMO receiver array with spectral–spatial mapping using one beamformer and single-wire interface," *IEEE J. Solid-State Circuits*, vol. 58, no. 5, pp. 1–13, Mar. 2023, doi: 10.1109/jssc.2023.3253793.

[47] E. C. Ifeachor and B. W. Jervis, *Digital Signal Processing—A Practical Approach*. Boston, MA, USA: Addison-Wesley, 1997.

[48] G. Wade, *Signal Coding and Processing*. Cambridge, UK: Cambridge Univ. Press, 1994.

[49] Analog Devices, Ltd. "ADG702 datasheet." Accessed: Apr. 30, 2023. [Online]. Available: https://www.analog.com/en/products/adg702.html

[50] Analog Devices, Ltd. "HMC374SC70E datasheet." Accessed: Apr. 30, 2023. [Online]. Available: https://www.analog.com/en/products/hmc374sc70e.html

[51] Analog Devices, Ltd. "LT5527 datasheet." Accessed: Apr. 30, 2023. [Online]. Available: https://www.analog.com/en/products/lt5527.html
[52] Analog Devices, Ltd. "AD8009 datasheet." Accessed: Apr. 30, 2023. [Online]. Available: https://www.analog.com/en/products/ad8009.html
[53] Texas Instruments, Ltd. "BUF602 datasheet." Accessed: Apr. 30, 2023. [Online]. Available: https://www.ti.com/product/BUF602
[54] S. Farzaneh and A.-R. Sebak, "Microwave sampling beamformer—Prototype verification and switch design," *IEEE Trans. Microw. Theory Techn.*, vol. 57, no. 1, pp. 36–44, Jan. 2009, doi: 10.1109/TMTT.2008.2009080.
[55] J. Jeong, N. Collins, and M. P. Flynn, "A 260 MHz IF sampling bit-stream processing digital beamformer with an integrated array of continuous-time band-pass $\Delta\Sigma$ modulators," *IEEE J. Solid-State Circuits*, vol. 51, no. 5, pp. 1168–1176, May 2016, doi: 10.1109/JSSC.2015.2506645.
[56] S. Jang, R. Lu, J. Jeong, and M. P. Flynn, "A 1-GHz 16-element four-beam true-time-delay digital beamformer," *IEEE J. Solid-State Circuits*, vol. 54, no. 5, pp. 1304–1314, May 2019, doi: 10.1109/JSSC.2019.2894357.
[57] L. Zhang, Y. Shen, L. De Vreede, and M. Babaie, "A 23.8-30.4-GHz vector-modulated phase shifter with two-stage current-reused variable-gain amplifiers achieving 0.23° minimum RMS phase error," *IEEE Solid-State Circuits Lett.*, vol. 5, pp. 150–153, 2022, doi: 10.1109/LSSC.2022.3179661.
[58] Y.-T. Chang and K.-Y. Lin, "A 28-GHz bidirectional active Gilbert-cell mixer in 90-nm CMOS," *IEEE Microw. Wireless Compon. Lett.*, vol. 31, no. 5, pp. 473–476, May 2021, doi: 10.1109/LMWC.2021.3061658.

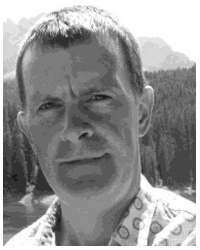

EDWARD A. BALL (Member, IEEE) was born in Blackpool, U.K., in November 1973. He received the Master of Engineering degree (First Class) in electronic systems engineering from the University of York, York, U.K., in 1996.

After graduating, he worked in industry for 20 years, first spending 15 years working as an Engineer, a Senior RF Engineer, and finally a Principal RF Engineer with Cambridge Consultants Ltd., Cambridge, U.K. He then spent five years as a Principal RF Engineer and a Radio Systems Architect with Tunstall Healthcare Ltd., Whitley, U.K. He joined the Department of Electronic and Electrical Engineering, The University of Sheffield, Sheffield, U.K., in November 2015, where he currently works as a Reader of RF Engineering. His research interests cover all areas of radio technology, from RF system design, RF circuit design (sub-GHz to mmWave), and the application of radio technology to real-world industrial and commercial problems. He has a particular passion for RF hardware design.

Mr. Ball is a member of IET and a Chartered Engineer.

SUMIN DAVID JOSEPH received the B.Tech. degree (Hons.) in electronics and communication from the Cochin University of Science and Technology, Cochin, India, in 2012, the M.Tech. degree (Hons.) in communication systems from the Visvesvaraya National Institute of Technology, Nagpur, India, in 2015, and the dual Ph.D. degrees (Distinction) in electrical engineering from the University of Liverpool, Liverpool, U.K., and National Tsing Hua University, Hsinchu, Taiwan, in 2021.

He is currently working as a Postdoctoral Research Associate with The University of Sheffield, Sheffield, U.K. He was a Lab Engineer under CoE with the Visvesvaraya National Institute of Technology from 2015 to 2017, where he was involved in projects of national importance. He has authored or coauthored more than 25 articles in peer-reviewed journals and conference proceedings. His research interests include self-biased circulators, mmWave antenna arrays, rectifying antennas, MMIC circuit design, RF circuit design, rectifiers, integrated circuit designs, flexible electronics, wireless power transfer, energy harvesting, and TMA antenna arrays.

Dr. David Joseph is a Technical Reviewer for leading academic journals and conferences, including the IEEE TRANSACTIONS ON ANTENNAS AND PROPAGATION, IEEE ANTENNA AND WIRELESS PROPAGATION LETTERS, and IEEE ACCESS.

ALAN TENNANT received the B.Eng. degree in electronic engineering and the Ph.D. degree in microwave engineering from The University of Sheffield, Sheffield, U.K., in 1985 and 1992, respectively.

He was with BAE Systems, Stevenage, U.K. He then joined DERA, Farnborough, U.K., where he worked on phased-array antenna systems before taking up an academic post with Hull University, Hull, U.K. He returned to The University of Sheffield in 2001 as a Senior Lecturer with the Communications and Radar Group, where he is currently a Professor and involved in research into techniques, materials, and signal processing for adaptive radar signature management, novel 3-D phased-array antenna topologies, acoustic array systems, and new research into time-modulated array antennas. He has published over 100 academic articles, including several invited articles on adaptive stealth technology. His research has attracted substantial funding from both industry and government sources.